Engineering and Technology Journal
Journal homepage: https://etj.uotechnology.edu.iq

The Structural and Optical Properties of Nanocrystalline Fe_3O_4 Thin Films Prepared by PLD

Khalid A. Abdulkareem, Suad M. Kadhim*, Shams B. Ali

Laser and Optoelectronics Engineering Dept., University of Technology-Iraq, Alsina'a street, 10066 Baghdad, Iraq.
*Corresponding author Email: Suad.M.Kadhim@uotechnology.edu.iq

HIGHLIGHTS

- Fe_3O_4 had a cubic spinel structure because of the strongest reflection from 311 planes.
- Increasing the pulse laser energy reduces the energy gap of films.
- When the pulses laser energy increases, the absorption and the film's thickness increase.

ARTICLE INFO

Handling editor: Ivan A. Hashim

Keywords:
X-Ray Diffraction (XRD)
Fe_3O_4
Iron Oxide
Magnetite
Optical properties
Pulsed Laser deposition

ABSTRACT

In this study, thin films of pure iron oxide (Fe_3O_4) were prepared using pulsed laser deposition technique under vacuum (2×10^{-3} mbar) using Nd: YAG laser at different laser energies (700, 800, 900, and 1000 mJ) on quartz slides at the substrate temperature of 200 °C with different thickness (170, 190, 220, and 250 nm). The prepared thin films were examined using different techniques. The X-ray diffraction showed a polycrystalline structure of cubic Fe_3O_4 phase, enhanced its crystallinity, and increased the crystalline size when increasing the laser energy to 1000 mJ. The results revealed that high transparency samples decreased pulse laser energy. As the laser pulse power increases, the transparency decreases from 91% to 61%, where optical properties deteriorate significantly. The bandgap values were detected to be 3.9 eV, 3.75 eV, 3.21 eV, and 3 eV when the laser energies were increased with thickness (170–250) nm. In addition, the extinction coefficient, dielectric constants, optical constants, and refractive constants were studied.

1. Introduction

Fe_3O_4 is one of the essential oxides because of its special unique magnetic properties. It has been widely studied recently. It has been used in a wide range of applications, such as sensors, medical, catalysts, electronic industries, solar cells, microwave absorbers, toxic heavy metal removal, etc., due to their physical and chemical properties as well as their unique magnetic properties, etc. [1-4]. The magnetic characteristics of Fe_3O_4 nanoparticles can be easily modified and improved by manipulating shape, particle size, crystal structure, and surface anisotropy [3].

Fe_3O_4 at room temperature has an inverted crystalline spinel structure [5] with Fd3m as the space group and a = 8.397 Å as the lattice parameter [1]. It contains Fe^{2+} and Fe^{3+} ions within the sub-lattice of oxygen and with a particular structure through which we can distinguish it from other iron oxides.

Magnetite features have high Curie temperature (TC~850K), high magnetic moment, semi-metallic, and non-toxic [6,7].

Several techniques exist to prepare Fe_3O_4 thin films, such as pulsed laser deposition, spraying, gel solution [4], molecular beam epitaxy, sputtering, metalorganic chemical vapor deposition, solid reaction [8], Screen printing, and Coating method (spin coating) [9]. The pulsed laser deposition technique is widely used to fabricate Fe_3O_4 thin films, and the final properties of the prepared samples can be tuned by altering the experimental parameters. In addition, many researchers examined the effect of different substrates on the physical properties of Fe_3O_4 films such as Si, MgO, and quartz [10].

The thin film is a nanometer-sized material created by arranging and incorporating atomic properties. The optical properties of thin films are heavily influenced by the energy gap that depends on the properties of the thin film material to be deposited [9].

In this study, the PLD method was used because it is simple, and the thin film is created in one step. Knowing that there is no research to make a Fe_3O_4 film by changing the energies of laser pulses so far, the results of Fe_3O_4 thin film have been shown, such as UV-VIS and X-ray diffraction (XRD) at different laser energy.

http://doi.org/10.30684/etj.v40i2.2235
Received 15 June 2021; Accepted 17 August 2021; Available online 25 February 2022
2412-0758/University of Technology-Iraq, Baghdad, Iraq

2. Materials

Pure powder of iron oxide (Fe_3O_4) nanoparticles was manufactured by US Research Nanomaterials, Inc (20 nm Assay), the substrate of quartz, distilled water, absolute Ethanol from Scharlau.

3. Experimental

The pure Fe_3O_4 powder with 5g was utilized to prepare the target for deposition as a pellet by hydraulic compressors at 7 tons for 7 minutes, as shown in Figure 1.

Figure 1: The pellet of Fe_3O_4 20 mm diameter and thickness of 6 mm

The rectangular quartz slides are commercially available with measurements (35×70) mm^2 and were used as a substrate. The substrate slide has been cut into pieces of (1.5×1.5) cm^2. They are subsequently cleaned for 10 minutes by alcohol with an ultrasound device, then for 12 minutes with distilled water, and finally dried by plowing air. From one step, the Fe_3O_4 thin films were deposited immediately upon quartz substrates with a pulse laser deposition technique (PLD). The deposition process was done within the PLD system's vacuum chamber at a pressure of 2×10^{-3} mbar. Next, the substrate and target were installed inside the vacuum chamber. The target was installed on a base that rotates during the work. The substrate is fixed at an angle of 45 degrees of a distance of 5 cm above the target. This is to ensure that particles excised from the surface of the target are directly deposited onto the substrate, as shown in Figure 2.

The laser beam was focused upon the target using a lens with a focal length of 12 cm. Laser Nd:YAG type (HF-301 from Huafei Technology made in China) was applied to Bombing the Fe_3O_4 target for constant pulses of laser (400 pulses) for each sample with various laser energies. Characteristics of the PLD system used and the parameters that were taken into account in this work are the wavelength of the laser 1064 nm, the pulse duration 10 ns, the laser energy 700, 800, 900, and 1000 mJ, the pulses frequency 6Hz, and the substrate temperature 200°C.

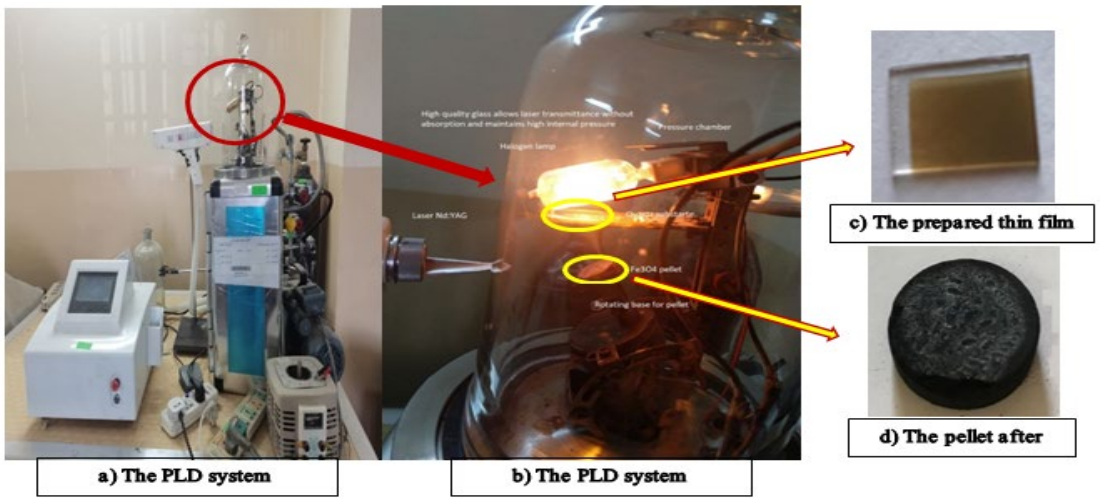

Figure 2: Preparing of Fe_3O_4 films at different laser energy (a,b,c, and d)

To find out the composition of the material, the degree of crystallinity, and the crystal structure, it is done using X-ray diffraction (XRD) (Shimadzu 6000-XRD) from (20-80 degrees) by wavelength 0.154056 nm. Then, the UV- visible absorptions for the thin films were measured using a double-beam UV-VIS SP-80001 spectroscopy device, by Scanning range from (190~1100nm) and StellarNet Inc SL1 determines the thickness.

4. Results and Discussion

4.1 X-ray diffraction analysis

X-ray diffraction was used to investigate the structural characteristic of Fe_3O_4 nanoparticles and the crystallinity of the resulting thin films. Bragg's law equation was used to calculate the interplanar distance (d_{hkl}) [11].

$$n\lambda = 2d_{hkl}sin\theta \quad (1)$$

where n: is a reflections order, λ is the falling X-ray wavelength and Θ: is the diffraction angle (Bragg's angle).
The crystal size C.S was studied by using Scherrer neutralization [12-14]:

$$C.S = K\lambda/\beta cos\theta \quad (2)$$

Where *K* is structure factor= 0. 93, β is the entire width of the peak at half maximum (FWHM).
The lattice constant (a) was evaluated for the preferred peak (311) by applying the relationship [13]:

$$a = d_{hkl}\sqrt{h^2 + k^2 + l^2} \quad (3)$$

Figure 3 shows the XRD patterns for the Fe_3O_4 powder, from which it can be deduced that Fe_3O_4 crystal has a cubic spinel structure due to the most substantial reflection along the (311) plane at 2θ=35.6456. The result agrees with the standard from the COD database of card no. (00-900-2318).

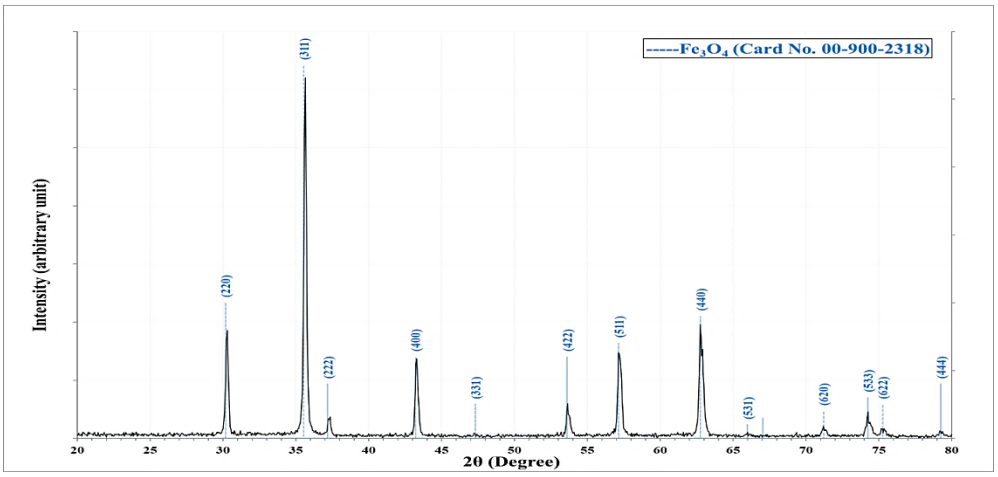

Figure 3: XRD pattern of Fe_3O_4 powder

Table 1 shows the structural parameters for the Fe_3O_4 powder. These parameters include the diffraction angles, full width at half maxima (FWHM), inter-planer spacing (d_{hkl}) calculated using Bragg's law, crystalline size (C.S) calculated using Sherrer's formula, and corresponding Miller indices for the peaks of diffraction.

Table 1: XRD for the Fe_3O_4 powder in comparison with the standard

2θ (Deg.)	FWHM (Deg.)	d_{hkl} Exp.(Å)	C.S (nm)	hkl
30.2925	0.2006	2.9481	41.0	(220)
35.6456	0.2382	2.5167	35.0	(311)
37.3255	0.2132	2.4072	39.3	(222)
43.2929	0.2507	2.0882	34.1	(400)
53.6481	0.2758	1.7070	32.3	(422)
57.1584	0.3134	1.6102	28.9	(511)
62.7622	0.3385	1.4793	27.5	(440)
71.1868	0.2758	1.3235	35.4	(620)
74.2457	0.2883	1.2763	34.6	(533)
75.2361	0.2632	1.2620	38.1	(622)
79.2353	0.3385	1.2080	30.5	(444)

Figure 4 shows the XRD pattern of Fe_3O_4 nanofilms prepared by PLD on quartz substrates with various laser energies starting from 700 mJ to 1000 mJ. Table 2 shows the XRD parameters of the thin Fe_3O_4 films.

According to the results of the XRD pattern, the effect of the laser power was revealed; the film prepared by 700 mJ laser energy appeared as amorphous, maybe because the laser energy is insufficient to cause the molecules to be arranged in a crystalline form. In comparison, the other samples were polycrystalline of a monoclinic structure. It was found that peaks intensity increases with increasing pulse laser energy which means an improvement in the crystal structure of the films, and this corresponds to the study of reference [15]. There are decreases in the width of the peaks (FWHM) from 0.327 to 0.221. Such behavior indicates an increase in the crystalline size of the particles (C.S) from 25.5 Å to 37.7 Å. These results were consistent with many kinds of research for the deposition of metals oxides by pulse laser energy [16]. When compared with [Card No. 00-900-2318), it was also observed that the experimental and standard parameters of (d_{hkl}) are in good agreement.

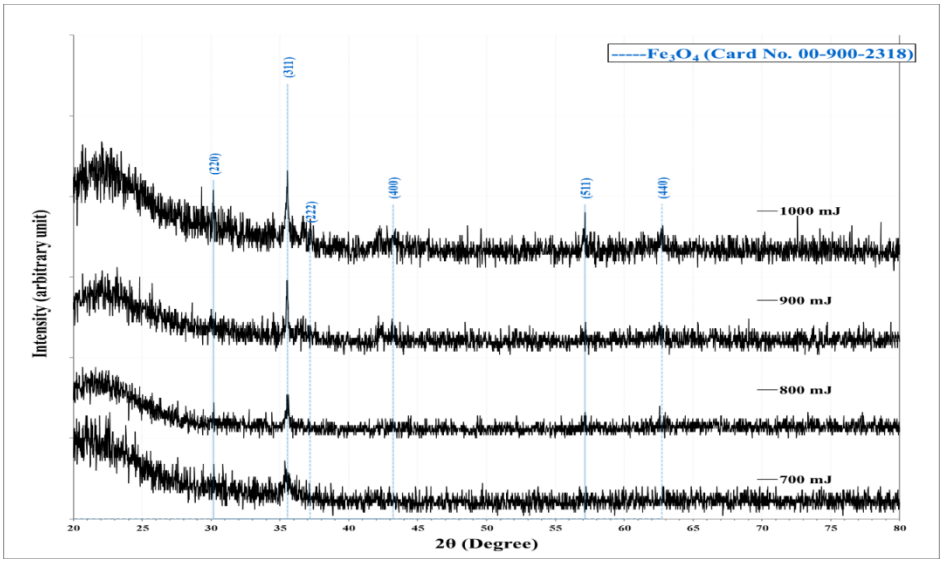

Figure 4: Fe_3O_4 thin films XRD pattern as a laser energy function

Table 2: X-ray parameters for Fe_3O_4 thin films prepared at various laser energy

Laser energy (mJ)	2θ (Deg.)	FWHM (Deg.)	d_{hkl} (Å)	C.S (nm)	hkl	a (Å)
700			Amorphous			-
800	35.6200	0.3270	2.5185	25.5	(311)	8.35279
	57.1444	0.4251	1.6106	21.3	(511)	
900	30.0054	0.3596	2.9757	22.9	(220)	8.36158
	35.5813	0.2289	2.5211	36.4	(311)	
	43.1499	0.3597	2.0948	23.7	(400)	
	56.9809	0.3597	1.6148	25.1	(511)	
1000	30.1362	0.3270	2.9631	25.2	(220)	8.36636
	35.5603	0.2274	2.5226	36.7	(311)	
	37.1989	0.1635	2.4151	51.3	(222)	
	43.1499	0.3269	2.0948	26.1	(400)	
	57.1444	0.1962	1.6106	46.1	(511)	
	62.7357	0.2943	1.4798	31.6	(440)	

4.2 Optical properties

The incident photon energy (hv) was computed with the formula (4) [17]:

$$E_g(eV) = 1.24 / \lambda\ (\mu m) \quad (4)$$

E_g is the optical energy gap, λ is the incident photon's wavelength.

The absorption coefficient was plotted as a function of wavelength, and the following equation was applied to calculate the energy gap [18,19]:

$$\alpha h\upsilon = A\ (h\upsilon - E_g)^r \quad (5)$$

Where (α) is the calculated absorption coefficient value, $h\upsilon$ is the photon energy ((h) is constant (Planck), (υ) is the frequency of photon), (A) is constant, (r) is a constant with values that depends on the type of the material and the energy gap. (E_g) was calculated by expanding the straight line of the $(\alpha h\upsilon)^2$ versus hυ plot.

Following eq. (6) has been applied to estimate the absorption coefficient at a specified wavelength [20,21]:

$$\alpha = 2.303\ (A/t) \quad (6)$$

A = absorptance and t = thickness of the thin film. The relation among the absorption α and extinction coefficient (K) can be obtained from Eq (7) [22]:

$$K = \frac{\alpha\lambda}{4\pi} \quad (7)$$

The index of refractive (n), the parts of dielectric of real (ε_r) and imaginary (ε_i), as well as optical conductivity (σ), could be derived from Eq. (8) [23]:

$$n = \{\frac{4R}{R-1} - K^2\}^{\frac{1}{2}} - \frac{R+1}{R-1} \quad (8)$$

Where (R) is reflectance that could be derived from ($R = 1 - T - A$). K is getting from Eq. (9) [24, 25]:

$$n = n_s \left(\frac{1+\sqrt{R}}{1-\sqrt{R}}\right)^{\frac{1}{2}} \quad (9)$$

n_s is the substrate refractive index. In this research, the substrate used in the deposition of thin films has 1.5 refractive indexes. Real (ε_r)and imaginary (ε_i) parts of dielectric constant are given by Eq [26, 27]:

$$\varepsilon = \varepsilon_1 - i\varepsilon_2 \quad (10)$$

And by using ($\varepsilon_r = n_2 - K_2$) and ($\varepsilon$ = 2nK). At last, an optical conductivity could be calculated using Eq. (11) [28]:

$$\sigma = \frac{\alpha nc}{4\pi} \quad (11)$$

Where c is the light speed.

The transmittance of Fe_3O_4 thin films was deposited with different thicknesses (170,190, 220, and 250) nm and with additional energy (700, 800,900, and 1000 mJ), as shown in Figure 5 (a). This is because the increase in film thickness means that the film absorption increases, resulting in a reduction in transmission [22]. It is observed from the figures that the optical transmittance value in the visible region was found to be increased slightly with decreasing the laser energy. The transmittance of the films appears to be a little stable at about 50% in the region (600-1000 nm). This is because of the effect of laser energy which tends to change the structure of the thin films' thickness and particle size [22].

In Figure 5 (b), the absorption spectrum of (200 to 1000) nm shows greater absorption characteristics of the treated sample with laser energies 1000 mJ, and the absorption peak position was at 232 nm. In contrast to the transmittance, the absorption coefficient has an inverse action. The α shows a high $X>10^4$ cm^{-1} value. Figure 5 (c) shows the absorption coefficient for various laser energies determined by Equation (6). All thin films have a different absorption coefficient. Films with larger values absorb incident photons more easily. This implies they induce electrons to move from valence band to conduction band. The larger values represent strong photon absorption at this wavelength, while the smaller values depict weak photon absorption at about this wavelength. The sharp point upon the absorption coefficient figure indicates insufficient energy in the material to move an electron from one level to the next. The absorption coefficient behaves similarly to absorbance. It can be noticed that the absorption coefficient will increase with increasing laser energies. This could be due to differences in the thickness of the films [22].

The energy band gap is depicted in Figure 5 (d). The bandgap is calculated by plotting $(\alpha h\nu)^2$ vs. hv and extrapolating a straight line to $(\alpha h\nu)^2=0$ [17]. The Free electrons number or/and defects with low energy of the incident photons can significantly impact the dielectric material's transmission spectrum. The results are nanocrystalline in the dimension of the Fe_3O_4 structure. These films are made by collecting crystals with random orientations and specific volumes, which affects the thickness of the sample. The energy gap decreased from 3.9, 3.75, 3.21and 3 eV when increasing laser energy from 700, 800, 900, and 1000 mJ, respectively. The sample of smaller crystalline size has a higher energy gap due to the effect of the quantum confinement phenomenon [29]. These values agree with previous studies about Fe_3O_4 nanoparticles [30].

Figure 5 (e) shows the relationship between refractive index and wavelength, measured by using relation (6). Refractive indices are affected by the wavelengths. Sample 900 mJ and 1000 mJ reach the maximum refractive index of 3.654011 and 3.65401 at 407 nm and 448 nm. Where the sample starts to increase in 700 mJ, first by the refractive index, then by 800 mJ, and reaches its maximum refractive index at 3.65401and 3.65401 at the wavelengths 252 nm and 292 nm, respectively, and then decreases the refractive index for them to stabilize to 1.60443 and 1.81005. Then, the refractive index decreases. Then, it decreases slightly and stabilizes where it was observed that the 1000 mJ sample with high thickness had the most extensive refractive index at stability, unlike the 700 mJ sample, which had a lower refractive index due to the small thickness.

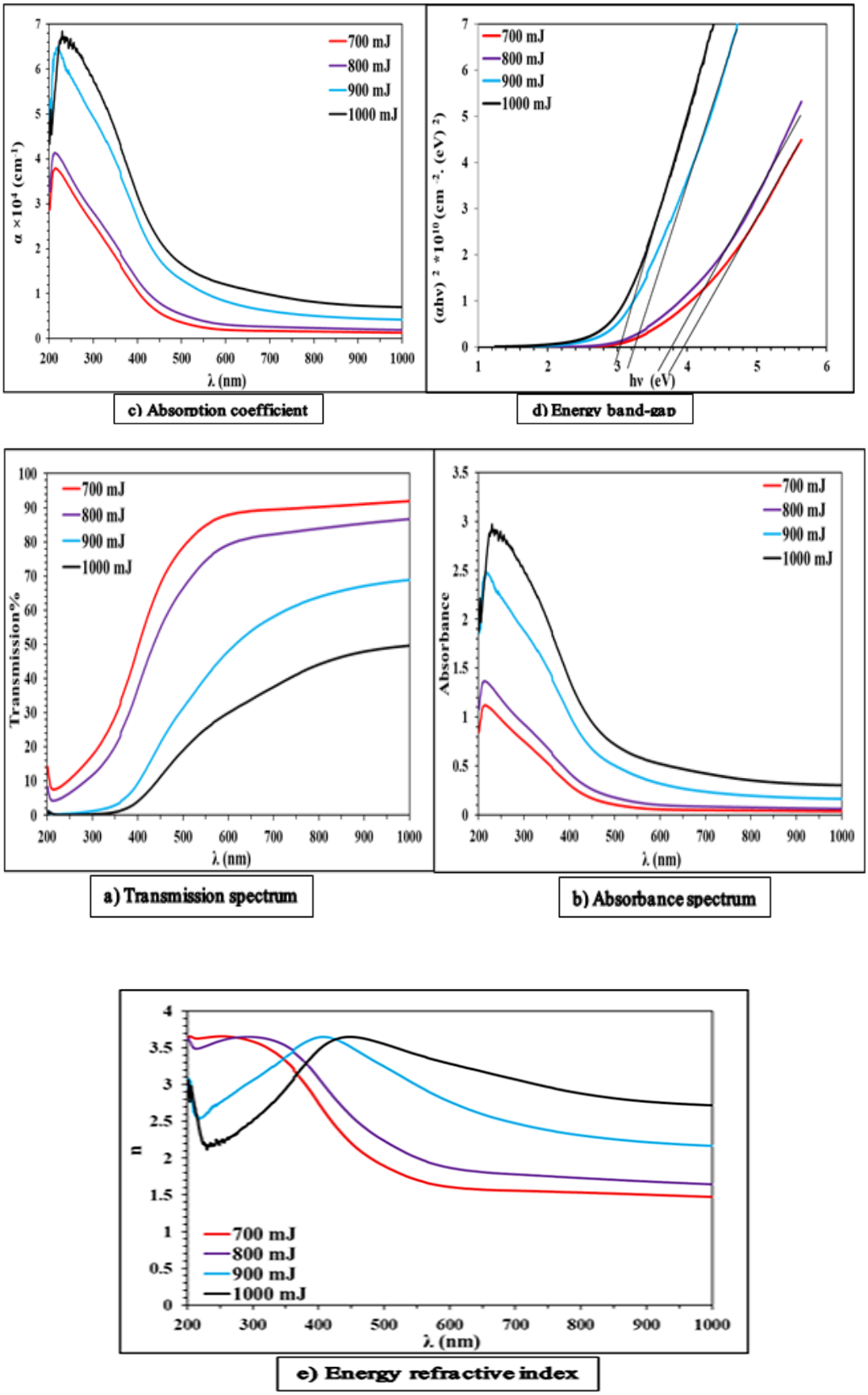

Figure 5: Fe_3O_4 film at different laser energy (a,b,c,d, and e)

Excitation coefficient (K) behaves in the same behavior of absorption coefficient (α); Figure 6 shows the coefficient of extinction (K) values vs. the energy of the incident photon at different laser power. Extinction coefficient increases with the increase of laser energy for all films. It is observed from these figures that the extinction coefficient, in general, decreased clearly with increasing wavelength until it reached its nearly constant values at 550 nm for all films until 1000 nm.

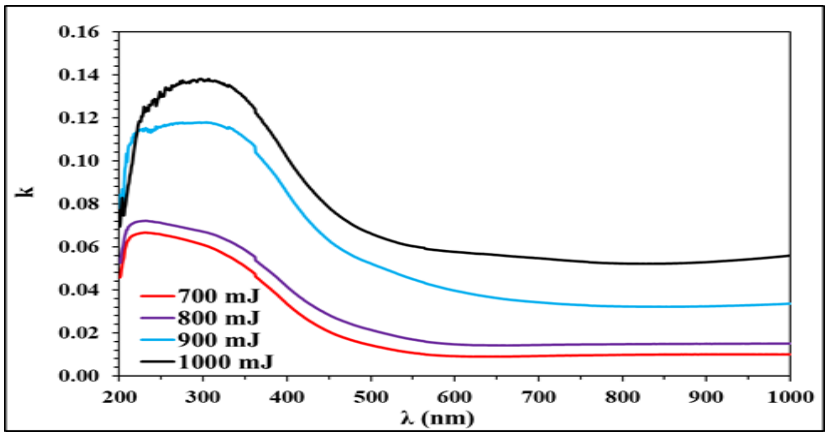

Figure 6: Extinction coefficient (K) of Fe_3O_4 thin films at different laser energy

While its imaginary part progressively increases to reach a certain point, the curve begins to change its behavior and decreases. The uniformity thickness of the samples causes this difference in optical properties, as shown in Figure 7 (b). The figure shows that the extinction coefficients of imaginary (ε_i) increased when the laser energy increased from 700 mJ to 1000 mJ for the deposited films. The action of n and k is generally the same as that of ε_r and ε_i, respectively [21].

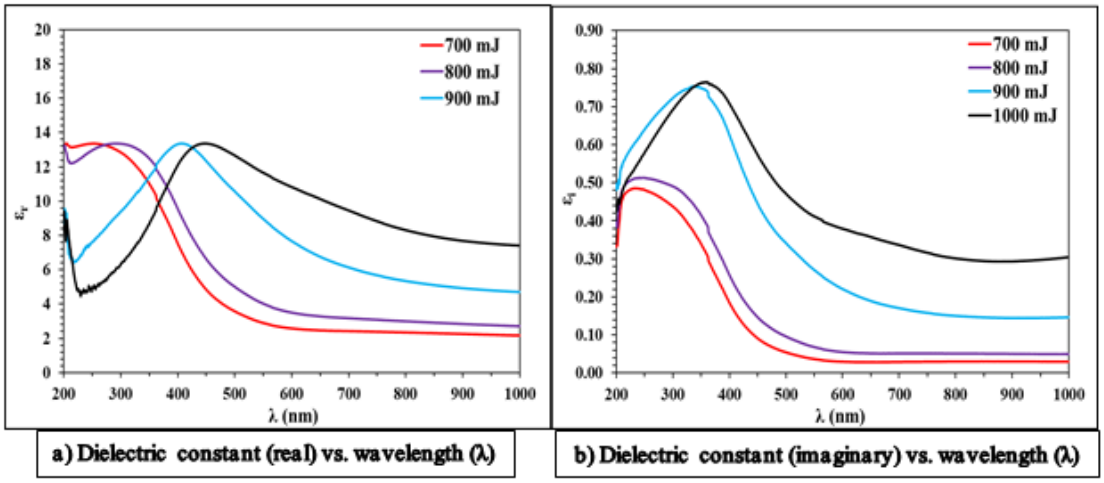

Figure 7: Fe_3O_4 at different laser energy

Table 3 shows the films' optical properties at the wavelength of 550 nm, which is in the middle of the visible spectrum. Moreover, Figure 8 depicts the effect of the pulse's laser energy on film thickness. A direct relationship between the thickness of the films and pulse laser energy is observed.

Table 3: The optical properties of the films at the wavelength 550 nm

Laser energy (mJ)	T%	α (cm^{-1})	K	n	ε_r	ε_i
700	84.74	2435	0.011	1.701	2.892	0.036
800	74.48	3878	0.017	2.003	4.014	0.068
900	40.37	10307	0.045	2.991	8.945	0.270
1000	25.26	13760	0.060	3.413	11.647	0.411

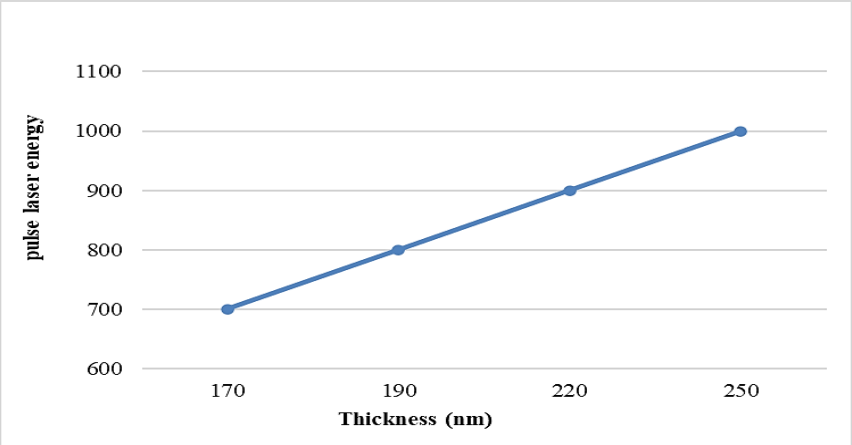

Figure 8: The thickness of Fe_3O_4 thin films for different pulse laser energies

5. Conclusion

Fe_3O_4 nanostructured thin films were physically prepared using the PLD technique by various laser energies. From the XRD results, the strongest reflection from 311 planes refers to the Fe_3O_4 having a cubic spinel structure. The laser energy pulse increases crystallization, peak intensity, and grain size increase about 43.922%. It was discovered that the prepared optical properties film at 700 mJ provides high transmission values (about 93%) for wavelengths higher than 600 nm and decreases with an increase in laser energy. The measured energy band gaps decrease with increasing the laser energy (3.9 eV, 3.75 eV, 3.21 eV, and 3 eV). The refractive index is also determined which the percentage increased at 550 nm wavelengths the refractive index increases about 100.647% at increased pulse energy. There is a direct relationship where the absorption, the absorption coefficient, and the thickness of the thin films increase about 47.06% with the increase in laser energy pulse.

Author contribution

All authors contributed equally to this work.

Funding

This research received no specific grant from any funding agency in the public, commercial, or not-for-profit sectors.

Data availability statement

The data that support the findings of this study are available on request from the corresponding author.

Conflicts of interest

The authors declare that there is no conflict of interest.

Reference

[1] X. Wang, Y. Liao, D. Zhang, T. Wen, Z. Zhong, A review of Fe3O4 thin films: Synthesis, modification and applications, J. Mater. Sci. Technol., 34 (2018) 1259–1272. http://dx.doi.org/10.1016/j.jmst.2018.01.011

[2] R. Suresh, K. Giribabu, R. Manigandan, L. Vijayalakshmi, A. Stephen, V. Narayanan, Electrochemical sensing property of Mn doped Fe 3 O 4 nanoparticles, AIP. Conf. Proc., 1512 (2013) 402–403. http://dx.doi.org/10.1063/1.4791081

[3] J. Mohapatra, A. Mitra, D. Bahadur, M. Aslam, Surface controlled magnetic properties of Fe3O4 nanoparticles, AIP. Conf. Proc., 1512 (2013). http://dx.doi.org/10.1063/1.4791039

[4] ABC. Ekwealor , E. Fabian, Effects of precursor concentration on the optical and structural properties of Fe2O3 thin films synthesized in a polymer matrix by chemical bath deposition, J. of Ovonic Res., 9 (2013) 35–43.

[5] R. Master, D. M. Phase, R. J. Choudhary, U. P. Deshpande, T. Shripathi, Fourier transform infrared study of pulsed laser deposited Fe3O4 thin films grown on different substrates, AIP. Conf. Proc., 1512 (2013) 724. http://dx.doi.org/10.1063/1.4791242

[6] D. Chen, S. Xiong, S. Ran, B. Liu, L. Wang, G. Shen, One-dimensional iron oxides nanostructures, Sci. China. Phys. Mec. Astr., 54 (2011) 1190–1199. http://dx.doi.org/10.1007/s11433-011-4372-3

[7] A. Roychowdhury, S. P. Pati, S. Kumar, D. Das, Magnetic-fluorescent nanocomposite: A case study on Fe3O4/ZnS, AIP Conf. Proc., 1512 (2013) 246. http://dx.doi.org/10.1063/1.4791003

[8] N. J. Tang, W. Zhong, H. Y. Jiang, X. L. Wu, W. Liu, Y. W. Du, Nanostructured magnetite (Fe_3O_4) thin films prepared by sol–gel method, J. Magn. Mag. Mate., 282 (2004) 92–95. http://dx.doi.org/10.1016/j.jmmm.2004.04.022

[9] N. Yulfriska, D. Rianto, F. Murti, Y. Darvina, R. Ramli, Optical Properties of Fe3O4Thin Films Prepared from the Iron Sand by Spin Coating Method, IOP. Conf. Ser. Mater. Sci. Eng., 335 (2018) 012010. http://dx.doi.org/10.1088/1757-899x/335/1/012010

[10] X. Huang, J. Ding, The structure, magnetic and transport properties of Fe3O4 thin films on different substrates by pulsed laser deposition, J. Korean Phys. Soc., 62 (2013) 2228–2232. https://doi.org/10.3938/jkps.62.2228

[11] W. H. Bragg , W. L. Bragg, X-rays , Crystal Structure G. Bell , sons, Limited, 1918).

[12] E. M. Nasir, Thickness and gamma-ray effect on physical properties of CdO thin films grown by pulsed laser deposition, Iraqi J. Phys., 14 (2019) 90–100. https://doi.org/10.30723/ijp.v14i29.225

[13] R. Jabbar, S. H. Sabeh, A. M. Hammed, Synthesis and Characterization of CoFe2O4 Nanoparticles Prepared by Sol-Gel Method, Eng. Tec. J., 38 (2020) 47–53. https://doi.org/10.30684/etj.v38i2b.252

[14] A. D. Faisal, M. A. Jaleel, F. Z. Kamal, Ethanol Gas Sensor Fabrication Based on ZnO Flower Like Nanorods, Eng. Tec. J., 38 (2020) 85–97. https://doi.org/10.30684/etj.v38i3b.279

[15] U. Jadhav, S. Gosavi, S. Patel, R. Patil, Archives of Physics Research, 2(2011) 27-35 .

[16] A. I. Khudiar , A. M. Ofui, Effect of pulsed laser deposition on the physical properties of ZnO nanocrystalline gas sensors, Opt. Mater., 115 (2021) 111010. https://doi.org/10.1016/j.optmat.2021.111010

[17] S. R. Elliott, Physics of amorphous materials. London; New York: Longman, (1984).

[18] S. M. Kadhim, Synthesis and Characteristic Study of Nanostructured (PbS/n-Si) by Chemical Bath Deposition, The Degree of Doctor of Philosophy (ph.D) in Appl. Phys., Departments of Appl. Sci. - University of technology, 2013.

[19] A. D. Faisal, M.A. Jaleel, F.Z. Kamal, Synthesis of ZnO Nanorods on Silicon for Methanol Gas Sensor, Eng. Tec. J. , 37 (2019) 74-81. https://doi.org/10.30684/etj.37.3B.2

[20] A. Abdulkhaleq Alwahib, S. F. Alhasan, M. H. Yaacob, H. N. Lim, M. A. Mahdi, Surface plasmon resonance sensor based on D-shaped optical fiber using fiberbench rotating wave plate for sensing pb ions, Optik, 202 (2020) 163724. https://doi.org/10.1016/j.ijleo.2019.163724

[21] Z. M. AL-Asady ,A. H. AL-Hamdani, Diffraction Rings Pattern and Nonlinear Optical Properties of Hybrid ZnO-NPs / Epoxy Resin, Eng. Tec. J. , 38 (2020) 440–445. https://doi.org/10.30684/etj.v38i3a.549

[22] E. M. Nasir, H. K. Al-Lamy, H. Abdul-Ameer, Optical Properties Of Cdse Films At Different Thickness And Annealing Temperatures, Chalcogenide. Lett.,16 (2019) 485–497.

[23] R. J. Elliott , A. F. Gibson, An introduction to solid state physics and its applications. Macmillan: London, 58 (1975). https://doi.org/10.1063/1.3068971

[24] D. Ciplys, R. Rimeika, I. Suarez, G. Lifante, M. S. Shur, A. Aulas, Guided-wave acousto-optic diffraction in Zn: LiNbO3, Electron. Lett., 42 (2006) 1294 – 1295. https://doi.org/10.1049/el:20061705

[25] V. Kumar, S. Kr. Sharma, T. P. Sharma, V. Singh, Band gap determination in thick films from reflectance measurements, Opt. Mater., 12 (1999) 115–119. https://doi.org/10.1016/s0925-3467(98)00052-4

[26] M. Caglar, S. Ilican, Y. Caglar, F. Yakuphanoglu, Electrical conductivity and optical properties of ZnO nanostructured thin film, Appl. Surf. Sci., 255 (2009) 4491–4496. https://doi.org/10.1016/j.apsusc.2008.11.055

[27] M.D. Femi, A. Ohwofosirai, A. Sunday, O.S. Ezema, R.U. Osuji, Variation of the optical conductivity dielectric function and the energy bandgap of CdO using cadmium acetate dehydrate, J. Mater .Sci., 2 (2014) 331– 337

[28] Sh. B. Ali, Deposition of lead sulfide (PbS) film and study of some of its physical properties, M.SC thesis in laser phys. Dep. of Appl. Sci. - University of technology, (2007).

[29] V. I. Klimov, Spectral and Dynamical Properties of Multiexcitons in Semiconductor Nanocrystals, Annu. Rev. Phys. Chem., 58 (2007) 635–673. https://doi.org/10.1146/annurev.physchem.58.032806.104537

[30] P. M. Kouotou, A. E. Kasmi, L.-N. Wu, M. Waqas, Z.-Y. Tian, Particle size-band gap energy-catalytic properties relationship of PSE-CVD-derived Fe3O4 thin films, J. Taiwan. Inst. Chem. Eng., 93 (2018) 427–435. https://doi.org/10.1016/j.jtice.2018.08.014